PCCP

PAPER

View Article Online
View Journal | View Issue

Cite this: *Phys. Chem. Chem. Phys.*, 2018, **20**, 23272

Stability of hydrolytic arsenic species in aqueous solutions: As^{3+} *vs.* As^{5+}

Giuseppe Cassone, *[a] Donatella Chillé,[b] Claudia Foti, *[b] Ottavia Giuffré,[b] Rosina Celeste Ponterio,[c] Jiri Sponer[a] and Franz Saija[c]

Received 9th July 2018,
Accepted 24th August 2018

DOI: 10.1039/c8cp04320e

rsc.li/pccp

Notwithstanding the fact that arsenic compounds are ubiquitous in the As^{3+} and As^{5+} forms in aqueous solutions, most of the microscopic features underlying the conditions of the hydrolysis steps are completely unknown. This way, a first-principles description of the fundamental behaviour of common arsenic species in natural waters and biological fluids is still lacking. Here we report on a synergistic computational and experimental investigation on As^{3+} and As^{5+} speciation in aqueous solution under both standard and sizably different alkaline circumstances. If, on the one hand, *ab initio* molecular dynamics simulations have been used to microscopically trace the different hydrolysis steps of As^{3+} and As^{5+} by explicitly taking into account the solvent contribution, on the other hand, they have been able to identify – and predict – the most stable hydrolytic species. In addition, by means of potentiometric and calorimetric measurements, the thermodynamic parameters ($\log K$, ΔH, and $T\Delta S$) have been determined at different ionic strength values ($0 < I \leq 1$ mol L^{-1}). By comparing the computational and the experimental findings of the species distribution under conditions of some biological fluids, a qualitative agreement on the compounds formed by As^{3+} and As^{5+} is thoroughly recorded and, therefore, the stable hydrolytic arsenic species present in natural waters and other biosystems are fully characterised.

1. Introduction

Arsenic is present in all the environmental compartments, atmosphere, soils, natural waters, as well as in the human body.[1,2] It stems indistinctly both from natural processes, such as weathering reactions and volcanic emissions, and from anthropogenic activities, including, *e.g.*, fossil fuels combustion, mining, ore smelting, well drilling, and its vast deployment in agriculture. Although it is found in inorganic and organic forms and in different oxidation states, the most widespread cationic species of arsenic are As^{3+} and As^{5+}.[3–7]

Since arsenic is a metalloid, it acts like a non-metal when it reacts with metals whereas it shows metal-like features when it reacts with non-metallic species. To this bivalent behaviour, a paradox in terms of its role in biological systems can be added. In fact, the International Agency for Research on Cancer (IARC) and the U.S. Environmental Protection Agency (EPA) classify arsenic as a human carcinogen;[8] it affects almost all vital organs of human body causing damages or dysfunctions such as dermatitis, cardiovascular diseases, diabetes mellitus, chronic bronchitis, immune disorders, and a plethora of side effects.[9] At the same time, however, arsenic has been and is still used as a therapeutic agent. In fact, it is well-known that Hippocrates and Paracelsus recommended arsenic for the treatment of some diseases whilst the ancient Chinese used arsenic trioxide as a drug for the treatment of various disorders. Moreover, Salvarsan (*i.e.*, an arsenic compound released in 1909) was the first important antisyphilitic drug. Recently, arsenic compounds have shown a remarkable therapeutic efficacy in patients with acute promyelocytic leukemia or other tumor forms.[10–14]

The harmful effect of As^{5+} is usually due to the similarity between the arsenate and the phosphate anions. Whereas in biological fluids arsenate may replace phosphate in some biochemical reactions – inhibiting thus the cellular processes – in natural waters and soils, phosphorus fertilizers promote its transport through direct desorption.[15,16] On the other hand, the toxicity of As^{3+} takes place through the interaction of trivalent arsenic species with sulfhydryl groups in proteins. Arsenite can form three-coordinated trigonal–pyramidal complexes with three cysteines, altering the conformation and the function of the protein itself. In this way, it disrupts the activity of certain enzymes.[17] The ability of arsenite to bind specific proteins is used to develop therapeutic and analytical applications such as *inter alia* cancer chemotherapy, molecular imaging,

[a] *Institute of Biophysics of the Czech Academy of Sciences, Královopolská 135, 61265, Brno, Czech Republic. E-mail: cassone@ibp.cz*
[b] *Dipartimento di Scienze Chimiche, Biologiche, Farmaceutiche ed Ambientali, Università di Messina, Viale F. Stagno d'Alcontres 31, 98166 Messina, Italy. E-mail: cfoti@unime.it*
[c] *CNR-IPCF, Viale Ferdinando Stagno d'Alcontres 37, 98158 Messina, Italy*

protein purification, and biosensing.[12,18,19] Recently, also quantum-based computational techniques have been invoked in order to unveil the typical behaviour of arsenic in its As^{3+} form, leading to arsenous acid (H_3AsO_3).[20] Although the latter studies reported interesting features of the hydrolysis steps of As^{3+} in water, the classical (*i.e.*, not-quantum) approach used in describing the key role held by the aqueous environment in assisting the resulting proton transfers fully neglected the quantum nature of the arsenic hydration shells. In addition, to the best of our knowledge, no *ab initio* molecular dynamics investigations – embedding thus an explicit treatment of the solvent – on As^{5+} in water have been reported so far.

With the aim of evaluating the reactivity and the biological activity of arsenic compounds under different natural and biological conditions and to unveil the microscopic behaviour of As^{3+} and As^{5+} cations in aqueous solutions, here we report on a combined computational and experimental investigation on those species in bulk water under different circumstances. On the one hand, we have employed *ab initio* molecular dynamics techniques in order to atomistically trace the distinct capabilities As^{3+} and As^{5+} hold during the hydrolysis steps in an aqueous environment both under standard and under sizably different alkaline conditions, a type of approach already proved to be highly predictive for proton transfer reactions.[21–24] On the other hand, potentiometric and calorimetric measurements have been performed to define typical thermodynamic parameters of the As^{3+} and As^{5+} hydrolysis under experimental conditions simulating ionic strength values of most natural waters and of biological fluids.

2. Methods

2.1. *Ab initio* molecular dynamics simulations

Five numerical samples of liquid water containing an As^{3+} species and five aqueous samples containing an As^{5+} one each have been placed in cubic super-cells and simulated under significantly different pH conditions. In particular, two simulation boxes contained one arsenic cation each (*i.e.*, one As^{3+} and one As^{5+}) surrounded by 128 neutral water molecules, accounting for a total of 385 atoms present in each simulation box. Two simulation cells contained one arsenic cation per type, 126 H_2O molecules, and 2 hydroxide (OH^-) anions each (*i.e.*, 383 atoms each). The remainder six simulation boxes (three per each arsenic cationic form) contained progressively lower/higher amounts of water/hydroxide species (*i.e.*, 124 H_2O and 4 OH^-, 122 H_2O and 6 OH^-, and 120 H_2O and 8 OH^-, respectively). Although the investigated alkaline conditions are certainly extreme, these circumstances have to be computationally reproduced in order to unveil – within the limited size and timescales affordable by accurate first-principles approaches – the different stable hydrolytic arsenic forms and achieve, thus, a qualitative comparison with the laboratory experiments. In addition, the quantity of the simulations (*i.e.*, 10), along with the size- and the time-lengths investigated in our calculations, represents a computational upper-bound for the most powerful super-computers. In fact, each cubic simulation box was characterised by an edge equal to 15.81 Å whereas trajectories of 20 ps have been carried out for each of the simulated samples with one exception: the trajectory of the simulation of As^{3+} in the presence of 128 water molecules has been propagated for longer times (*i.e.*, 100 ps) in order to check whether the characteristic time for the third hydrolysis step (τ_3) can be appreciated within timescales affordable by *ab initio* molecular dynamics (MD) simulations. The latter is the subject of a heated debate.[20,25,26] As usual, all the structures were replicated in space by means of periodic boundary conditions.

We used the software package CP2K,[27] based on the Born–Oppenheimer approach, to perform *ab initio* MD simulations of all the above-mentioned samples. Electronic wave-functions of each atomic species have been expanded on double zeta valence plus polarization (DZVP) basis sets. As for exchange and correlation (XC) effects, we adopted the gradient-corrected Becke–Lee–Yang–Parr (BLYP)[28,29] functional in conjunction with D3(BJ) Grimme's dispersion corrections,[30,31] whereas Goedecker–Teter–Hutter[32] pseudopotentials have been chosen to mimic the core electronic interaction. A cutoff energy for wave function representation of 40 Rydberg (Ry) and a cutoff of 400 Ry for charge density have been employed whereas a timestep of 0.5 fs, typical for Born–Oppenheimer MD, has been chosen. All the *ab initio* MD simulations have been carried out at the average temperature of 300 K kept fixed through the velocity rescaling method.[33] In this way, samples were simulated in an isothermal–isochoric (*NVT*) ensemble and the dynamics of the nuclei was classically propagated using the Verlet algorithm.

2.2. Experiments

2.2.1. Reagents. Arsenic(III) solution was prepared by weighing the sodium (meta)arsenite salt (Sigma-Aldrich, $\geq$90%). Sodium hydroxide and hydrochloric acid solutions were prepared from concentrated Fluka ampoules and titrated with potassium biphthalate and sodium carbonate (dried in an oven at 110 °C for at least an hour), respectively. NaOH was stored in dark bottles and preserved by CO_2 by means of soda lime traps. Sodium chloride solution was prepared by weighing the corresponding salt (Fluka, puriss.) pre-dried in an oven at 110 °C. All the solutions were prepared with analytical grade water (conductivity <0.1 μS cm^{-1}) and using grade A glassware.

2.2.2. Potentiometric equipment and procedure. The potentiometric technique was employed to determine the protonation constants of As^{3+} cation. In order to minimize the systematic errors, potentiometric measurements were independently performed by two operators using different reagents and two different systems: (i) A Metrohm model 809 Titrando potentiometer equipped with an Orion-Ross 8102 combined glass electrode and an automatic dispenser Metrohm Dosino 800. The automated titration system is interconnected with a PC which, by employing a specific software named TIAMO 2.2, is able to control e.m.f. stability, titrant delivery and data acquisition. (ii) A Metrohm 713 potentiometer, equipped with a half cell glass electrode (Ross type 8101, from Thermo/Orion)

combined with a double-junction reference electrode (type 900200, from Thermo-Orion), and a 765 Metrohm motorized burette. The system was connected to a PC and automatic titrations were performed using a suitable homemade computer program to control titrant delivery, control data acquisition and to check for e.m.f. stability.

The estimated reproducibility was ±0.15 mV, for the e.m.f., and ±0.003 mL, for titrant volume readings. The measurement cells were thermostated at the prefixed temperature (273.15 ± 0.1) K by means of water circulation from a thermocryostat (mod. D1-G Haake). Purified N_2 was bubbled through the solution to exclude O_2 and CO_2.

To determine the protonation constants, a volume of 25 mL of the solution containing the arsenite salt ($1 \leq C_L$/mmol $L^{-1} \leq 6$), HCl ($5 \leq C_{HCl}$/mmol $L^{-1} \leq 10$) and NaCl as background salt at different ionic strength values ($0.1 \leq I$/mol $L^{-1} \leq 1$) was titrated with standard NaOH in the $2 \leq$ pH ≤ 11 range. Independent experiments were performed at least three times.

For each experiment, independent titrations of strong acid (HCl) solutions with carbonate-free NaOH solutions were carried out under the same temperature and ionic strength conditions as the systems to be investigated with the aim of determining the electrode potential (E^0) and the acidic junction potential ($E_j = j_a$ [H^+]). In this way, the free proton concentration scale was used, pH ≡ $-\log_{10}[H^+]$, where [H^+] is the free proton concentration. The reliability of the calibration in the alkaline range was checked by calculating the ionic product of water (pK_w).

2.2.3. Calorimetric equipment and procedure. The calorimetric technique was employed to determine the protonation enthalpy of As^{3+} cation. Measurements were performed using an isoperibolic titration calorimeter CSC (Calorimetry Science Corporation), model 4300, at 273.150 ± 0.001 K. The titrant was dispensed by a 2.5 mL capacity Hamilton syringe, model 1002TLL, and a specific computer program was used to acquire, automatically, calorimetric data. The solution from syringe was delivered continuously with an injection speed of 0.1 mL min^{-1}. Before each experiment the heat of dilution was measured. The system accuracy was verified by titrating a tris-(hydroxymethyl)aminomethane buffer solution with HCl and determining, for each experiment, the heat of dilution. The precision of calorimetric apparatus was Q ± 0.015 J and v ± 0.001 mL.

For the enthalpy determination, a volume of 25 mL of the solution containing the arsenite salt (20 mmol L^{-1}) and NaCl, as background salt at different ionic strengths ($0.1 \leq I$/mol $L^{-1} \leq 1$), was titrated with HCl (1 mol L^{-1}). Calorimetric titrations were performed in the range $3.2 \leq$ pH ≤ 10.5.

2.2.4. Speciation programs. Parameters related to the electrode system calibration (formal potential E^0 and liquid junction potential coefficient j_a, $E_j = j_a$ [H^+]), the purity of the reagents, and the formation constants were determined using BSTAC and STACO computer programs. Calorimetric data were analysed by the ES5CM99 program. Dependence of formation constants on the ionic strength was studied using the LIANA program. Details on computer programs are reported in ref. 34. To calculate the species formation percentages and to draw the distribution diagrams, the HYSS program[35] was employed. Unless otherwise specified, uncertainties are given at a ±95% confidence interval (c.i.).

3. Computational results

Depending on the nature of the investigated arsenic form (*i.e.*, As^{3+} or As^{5+}), a different number of hydrolysis steps is expected upon water solvation of those cations in their bare state. In particular, a total of three steps can be theoretically predicted for As^{3+} whereas the situation may become less trivial for the As^{5+} case where, however, four hydrolysis steps are expected under standard conditions. The situation gets clearly more intricate when considering sizably different concentrations of the hydroxide anions present in the aqueous environment (*i.e.*, at different alkaline pH) where arsenic is dissolved.

As shown in Fig. 1a and 2, the first arsenic-induced water dissociation, in a sample containing As^{3+} and neat neutral water, takes place on timescales which are challenging to be experimentally explored (*i.e.*, 65 fs). Once the proton is released, it rapidly migrates along the water H-bonded network through the well-known Grotthuss mechanism. Although this value slightly differs from that estimated by Canaval and co-workers[20] (*i.e.*, 144 fs), it is adherent with that found in a Car–Parrinello simulation conducted by Coskuner *et al.* (*i.e.*, 60 fs).[36] However, a precise assessment of the real characteristic time of the first hydrolysis step (τ_1) of As^{3+} from numerical experiments is too strictly dependent on the peculiar starting configuration in

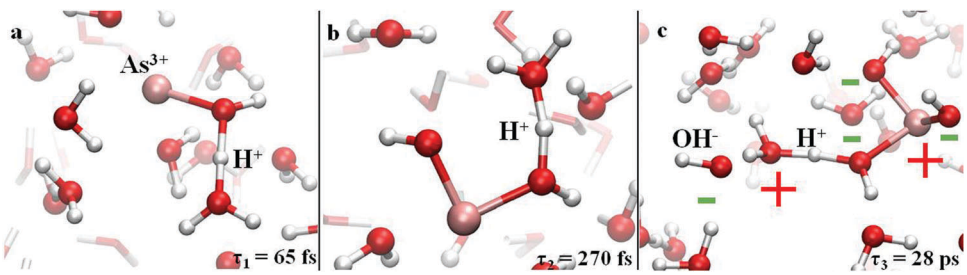

Fig. 1 First (a), second (b), and third (c) hydrolysis step mechanism taking place in a neutral aqueous solution where As^{3+} is dissolved, giving rise to arsenous acid. Red, white, and pink spheres represent oxygen, hydrogen and arsenic atoms, respectively. In (c) the signs indicate the local charge established once the proton transfer has taken place, stabilizing the adjacent water counter-ions.

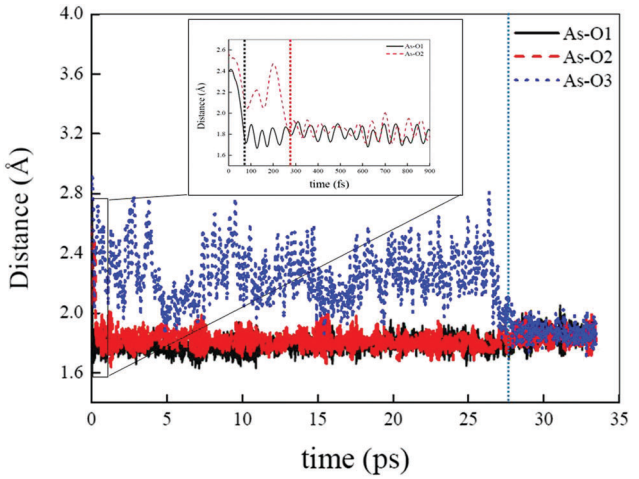

Fig. 2 Distances between the arsenic atom and the three oxygen atoms giving rise to the arsenous acid species plotted as a function of time. Vertical lines mark the characteristic times corresponding to the molecular configurations depicted in Fig. 1. Because of the deeply different time-scales on which the first two and the third hydrolysis steps occur, a magnification of the distances – during the first 900 fs of dynamics – between As^{3+} and the first two water oxygens leading to the transient $[As(OH)_2]^+$ complex is shown in the inset.

which the water molecules of the arsenic solvation shells lie. On the other hand, a more robust comparison can be made between distinct computational formalisms for the second characteristic time (τ_2). In fact, as depicted in Fig. 1b and 2, a typical time of 270 fs can be ascribed to such a process, similar to that found elsewhere within a QM/MM scheme[20] and that obtained at the Hartree–Fock level of theory in a QMCF-MD simulation.[27]

Water solvation shells play a major role in assisting the complex network of proton transfers that is at the base of each of the hydrolysis steps. This is particularly true for the last (the third) step taking place in an aqueous solution where an As^{3+} is dissolved. In fact, longer times – extending up to the ps time-scale – are necessary for the final step leading to the synthesis of the stable arsenous acid (H_3AsO_3). Notwithstanding recent computational estimates[20] indicate that τ_3 falls at approximately 12 ps, other calculations did not observe the third hydrolysis step either after 15 ps[26] or after 20 ps,[25] thus indicating longer timescales for the typical final hydrolysis step under standard conditions. The fact that our state-of-the-art *ab initio* MD revealed that the third hydrolysis step occurs at $\tau_3 \approx 28$ ps, as shown in Fig. 1c and 2, only partially strengthens the conclusions of Bhattacharjee *et al.*[26] and Hofer *et al.*[25] in spite of those reached by Canaval and co-workers that claimed a $\tau_3 \approx 12$ ps.[20] In fact, in all such literature,[20,25,26] the results have been achieved by means of hybrid QM/MM simulations where the radii of the quantum mechanical zone assumed values of 5.7 Å, enabling "a full quantum mechanical treatment of the arsenic ion, its ligands and the first hydration shell of the complex".[20]

Notwithstanding the authors of ref. 20 claim that the exact treatment of the electronic correlation allows for the correct evaluation of τ_3, it is so far more likely that the parametrized (*i.e.*, by means of classical *ad hoc* functions) treatment of the water molecules – as well as of the H_3O^+ species – and of the electrostatics of the problem for distances larger than 5.7 Å (from As^{3+}) renders too artificial a process that involves intrinsically quantum multiple and coordinated proton transfers occurring on sizably longer lengths and across several hydration shells.

Within a full first-principles scheme, we do suggest that the characteristic time of the third hydrolysis step in the presence of As^{3+} is around 28 ps. As shown in Fig. 1c, the formation of a hydroxide anion in one of the solvation shells of the arsenic complex $[As(OH)_2]^+$ is necessary in order to trigger a proton transfer between two water molecules present between the latter complex and the OH^- species. This way, the formation of the stable arsenous acid molecule has been achieved. Curiously, because of the electrostatic stabilization induced by the presence of alternating charged layers (see Fig. 1c), the further proton transfer between the two adjacent water counter-ions (*i.e.*, H_3O^+ and OH^-) is ultra-slow, occurring in about 4 ps, a value one order of magnitude larger than the typical neutralization events in water. Albeit unusual, the electric-field-induced stabilization of charged intermediate or transition states is a very well-established phenomenon.[37,38]

The situation dramatically changes when arsenic in the As^{5+} form is dissolved in bulk neutral water. Because of the higher charge and hence of its more Lewis-acidic character, the characteristic times of the hydrolysis steps are restricted with respect to the case of As^{3+} and all the successive proton transfer events can be appreciated within a few ps.

As shown in Fig. 3a and 4, the first hydrolysis event occurs after 60 fs, similar to the previous case. Somewhat surprisingly, the characteristic time for the second step is almost twice (Fig. 3b) than that recorded in the As^{3+} sample, suggesting that more complex interactions – than the bare electrostatic one – rule the overall hydrolysis process. Indeed, before reaching the $[As(OH)_2]^{3+}$ state (Fig. 3b), several attempts of water dissociation

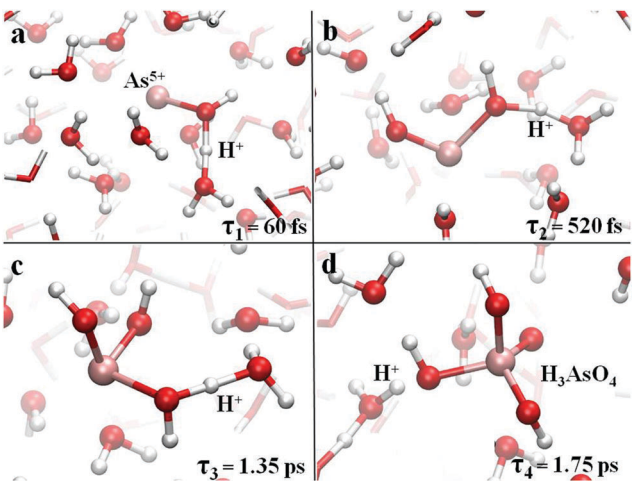

Fig. 3 Successive hydrolysis mechanisms taking place in a neutral aqueous solution where As^{5+} is dissolved. Red, white, and pink spheres represent oxygen, hydrogen and arsenic atoms, respectively.

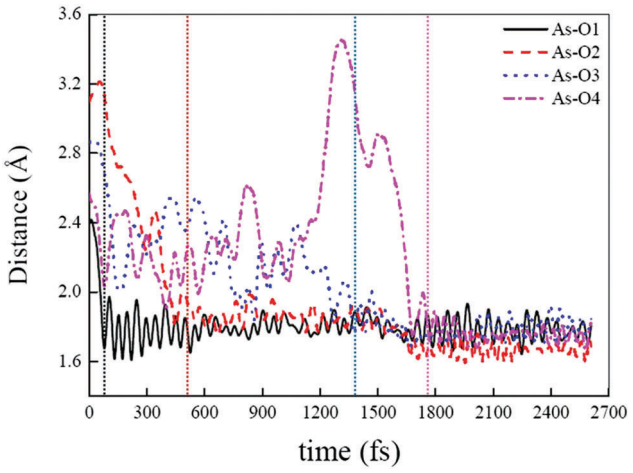

Fig. 4 Distances between the arsenic atom and the four oxygen atoms giving rise to the stable arsenic acid H_3AsO_4 plotted as a function of time. Vertical lines mark the characteristic times corresponding to the molecular configurations depicted in Fig. 3.

are induced by the transient ionic complex $[As(OH)]^{4+}$ in its first solvation shell. Similarly, disparate proton transfer attempts have to be statistically accumulated before reaching, after 1.35 ps, the complex which represents the direct precursor of the stable one (Fig. 3c). This way, in less than 2 ps the final stable product H_3AsO_4 (*i.e.*, arsenic acid) is reached (Fig. 3d) thanks to a cooperative mechanism that allows for the H^+ release from the oxygen involved in the second hydrolysis step.

In order to check whether the presence of hydroxide species allows for the prediction of the stable hydrolytic compounds formed by As^{3+} and As^{5+}, two pairs of OH^- anions have been added in each of the respective numerical samples. If in the previous As^{3+} case the last hydrolysis step has been observed only after 28 ps, in the presence of two hydroxide ions the typical timescale of such a process decreases by more than one order of magnitude. In fact, in addition to a sizable reduction of the characteristic time of the first two steps, the third one takes place just after 1.5 ps (3rd column of Table 1). Moreover, the latter value dramatically drops at 130 fs – indicating an ultrafast protonic re-organization – when in the As^{3+} sample are added two more OH^- species (4th column of Table 1) or four additional hydroxide anions (5th column). As a consequence of the extremely alkaline nature of the latter numerical sample, after 1.4 ps the transient arsenous acid evolves into a di-hydrogen arsenite species ($H_2AsO_3^-$) that represents the final stable hydrolytic species under such a condition. The latter conclusion has been independently confirmed by additional simulations performed with H_3AsO_3 in aqueous solution in the presence of some hydroxide species; it turned out that the formation of di-hydrogen arsenite spontaneously followed. Moreover, somehow counter-intuitively, a tightening of the alkaline conditions has not produced the formation of more negatively charged compounds such as, *e.g.*, $HAsO_3^{2-}$.

Table 1 Characteristic time (in fs) for the different hydrolysis steps of As^{3+} and As^{5+} under significantly different conditions of basic pH. The alkaline conditions marked as "low", "mild", and "high" refer to numerical samples where two, four, and six hydroxide ions are present, respectively

	As^{3+}				As^{5+}			
	Neutr.	Low	Mild	High	Neutr.	Low	Mild	High
τ_1 (fs)	65	40	20	20	60	50	50	50
τ_2 (fs)	270	100	50	50	520	60	50	50
τ_3 (fs)	28 000	1500	130	130[a]	1350	350	150	120
τ_4 (fs)	n.a.	n.a.	n.a.	n.a.	1750	800	400[b]	350[b]

[a] After 1.4 ps, an OH^- of the complex releases an H^+ and the stable product becomes $H_2AsO_3^-$. [b] Under such conditions the stable form is $H_2AsO_4^-$ and thus τ_4 represents the time necessary to reach the arsenic acid state before losing one H^+.

As far as the As^{5+} case is concerned, a significant reduction of all the four characteristic times associated with the hydrolysis steps has been recorded with increasing alkaline conditions of the solution, as shown in the right part of Table 1. More importantly, the most stable complex is di-hydrogen arsenate ($H_2AsO_4^-$) under both conditions defined here as "mild" and "high", where four and six hydroxide anions were present, respectively. In addition, on further increasing the pH of the solution (*i.e.*, by adding two or four OH^- species to the sample under "high" alkaline conditions), other two species are finally produced: hydrogen arsenate ($HAsO_4^{2-}$) and the arsenate anion (AsO_4^{3-}). The latter evidence clearly suggests that in a laboratory experiment performed at relatively high levels of alkalinity, those species statistically represent a relevant – or at least a detectable – fraction of the different complexes that As^{5+} is able to form in aqueous solutions.

4. Experimental results

As it has been shown, As^{3+} and As^{5+} cations behave quite differently in aqueous solution. As far as As^{3+} is concerned, in dilute water solutions, its most stable species is the arsenous acid H_3AsO_3. In fact, the main protonation equilibrium in which H_3AsO_3 is involved, at the pH values of natural waters, is[39]

$$H^+ + H_2AsO_3^- = H_3AsO_3^0 \quad (1)$$

The other equilibria concerning $HAsO_3^{2-}$ and AsO_3^{3-} occur at very high pH values[39] and so they are not of interest for natural waters. In effect, experimental potentiometric titrations performed in the $2 \leq pH \leq 11$ range and at metal concentrations between 1 and 6 mmol L^{-1} are in agreement with the single protonation equilibrium (1). Equilibrium constant values obtained by processing the experimental data through the BSTAC program are reported in Table 2 in NaCl for different ionic strength conditions.

As it can be observed, the increase of the ionic strength from 0.1 to 1 mol L^{-1} induces a decrease of the protonation constant, with $\log K$ that varies from 9.124 at I = 0.111 mol L^{-1}, to 9.021 at I = 0.971 mol L^{-1}. In order to model the ionic strength dependence, the following Debye–Hückel-type equation is used:

$$\log K = \log K^0 - 0.51 z^* \frac{\sqrt{I}}{1 + 1.5\sqrt{I}} + CI \quad (2)$$

Table 2 Experimental protonation constant values of As^{3+} in NaCl at different ionic strengths ($0.1 \leq I \leq 1$ mol L^{-1}) and at T = 298.15 K and the calculated one at infinite dilution

I/mol L^{-1}	$\log K^a$
0.111	9.124 ± 0.003^b
0.247	9.059 ± 0.002
0.494	9.028 ± 0.002
0.971	9.021 ± 0.002
0	$\log K^0 = 9.331 \pm 0.006^c$
	$C = 0.097 \pm 0.009^c$

[a] K refers to equilibrium: $H^+ + H_2AsO_3^- = H_3AsO_3^0$. [b] ±3 std. dev. [c] Calculated values by eqn (2).

where $z^* = \Sigma(\text{charges})^2_{\text{reactants}} - \Sigma(\text{charges})^2_{\text{products}}$, K is the formation constant, K^0 is the formation constant at infinite dilution, and C is an empirical parameter which depends on the charges involved in the formation reaction. From eqn (2) and the experimental values of $\log K$, the protonation constant at infinite dilution (K^0) and the parameter C are determined, as reported in Table 2. This way, from K^0 and C it is possible to evaluate the protonation constant values at various ionic strengths and therefore to simulate the distribution under conditions different from those experimentally probed. In fact, the good predictive power of eqn (2) has already been extensively tested for a wide number of acid–base and metal–ligand systems.[40–43]

The effect of ionic strength on species distribution is shown in Fig. 5 where, for comparison, the distribution at I = 0.1 mol L^{-1} and I = 0.97 mol L^{-1} is reported (blue and red lines, respectively). It turns out that the increase of the ionic strength produces a shift of the formation curves towards lower pH values. In all the cases, As^{3+} is present in solution as H_3AsO_3 up to pH ≈ 7. Beyond this threshold, the deprotonation process is triggered and between 7 < pH < 11 the coexistence of H_3AsO_3 and $H_2AsO_3^-$ species can be observed and, in the investigated pH range, no further deprotonation steps have been observed,

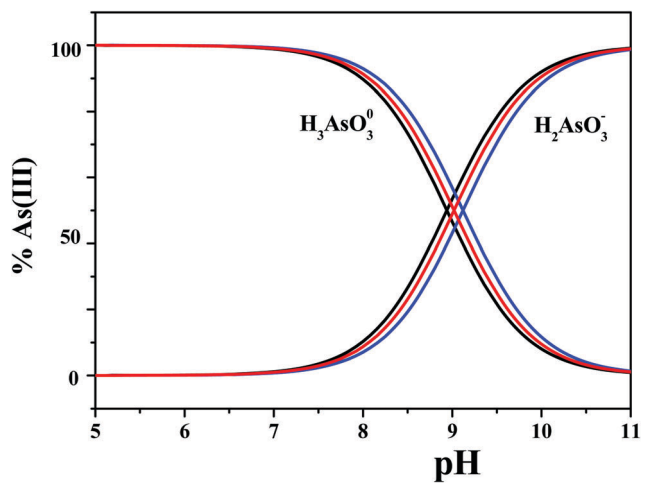

Fig. 5 Distribution diagram for As^{3+} species in NaCl under different experimental conditions (C_M = 1 mmol L^{-1}). Blue lines: I = 0.1 mol L^{-1}, T = 298.15 K; red lines: I = 0.97 mol L^{-1}, T = 298.15 K; black lines: I = 0.1 mol L^{-1}, T = 310.15 K.

as previously indicated by our *ab initio* MD simulations under alkaline conditions. Moreover, our first-principles molecular dynamics simulations have demonstrated that even under more extremely alkaline environments arsenite $H_2AsO_3^-$ species represents the stable compound formed by As^{3+}, further toughening *a posteriori* the reported experimental evidence.

With the aim of fully investigating the thermodynamic picture of the systems under study and to evaluate the effects of temperature on the protonation equilibrium, the formation enthalpy has been determined by titration calorimetry, as for several other systems.[44,45] The measurements have been performed at T = 298.15 K and in NaCl at three ionic strength values: I = 0.1, 0.5, and 0.7 mol L^{-1}. The respective results are listed in Table 3 along with the calculated ΔG (from potentiometric measurements) and $T\Delta S$ values.

Since the enthalpy change protonation value under all the ionic strength conditions is exothermic and its absolute value is similar to $T\Delta S$, the main contribution to the Gibbs free energy does not stem from the entropy itself. This is likely due to the presence of the protonated hydroxyl groups on As^{3+} cation, which may cause some loss of rotational freedom.

By using the Van't Hoff equation, the enthalpy change allows for the determination of the constants at different temperatures. The negative enthalpy value determines a decrease of the protonation constant as the temperature increases. This causes, in turn, a displacement of the species distribution towards lower pH values, as can be easily observed by comparing the curves shown in Fig. 5 at the same ionic strength, but for different temperatures (black and blue lines).

The protonation constant evaluation at different ionic strengths and temperatures is central for applications to real systems such as biological fluids and natural waters, having variable composition, ionic strength, pH, and temperature. Just to highlight the need to take into account ionic strength and temperature, notwithstanding the change of $\log K$ appears to be negligible, we report, in Fig. 6, some examples of the As^{3+} distribution in some common natural fluids: blood (in which I = 0.15 mol L^{-1}, T = 310.15 K, pH = 7.4), sea water (I = 0.7 mol L^{-1}, T = 298.15 K, pH = 8.1), and fresh water (I = 0.001 mol L^{-1}, T = 298.15 K, pH = 5). As can be observed, in fresh water, As^{3+} is present as entirely protonated, whereas in sea water and mostly in blood, the percentage of deprotonated $H_2AsO_3^-$ increases and reaches 11%. This evidence can clearly influence the behavior of As^{3+} in these fluids and, in particular, its complexing ability and its further interactions with other additional components.

Table 3 Thermodynamic formation parameters for arsenous acid in NaCl at different ionic strengths and at T = 298.15 K

I/mol L^{-1}	$\Delta H^{a,b}$	$-\Delta G^{a,b}$	$T\Delta S^{a,b}$
0.1	-26.5 ± 0.3^c	52.04 ± 0.02^c	25.5 ± 0.3^c
0.5	-30.1 ± 0.3	51.51 ± 0.01	21.4 ± 0.3
0.7	-23.2 ± 0.4	51.45 ± 0.01	28.2 ± 0.4

[a] ΔH, ΔG, and $T\Delta S$ refer to equilibrium: $H^+ + H_2AsO_3^- = H_3AsO_3^0$. [b] In kJ mol^{-1}. [c] ±3 std. dev.

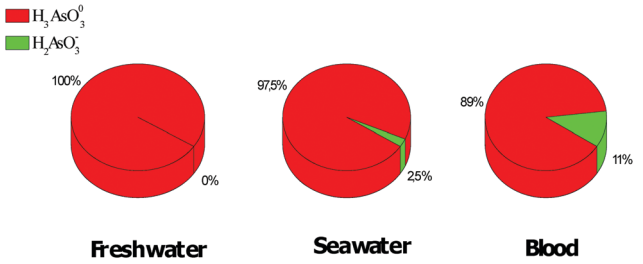

Fig. 6 Examples of As^{3+} distribution in some natural fluids.

The behaviour of As^{5+} is deeply different from that of As^{3+}. According to the first-principles computational results previously reported, the stable species H_3AsO_4 is involved in three protonation steps:

$$H^+ + AsO_4^{3-} = HAsO_4^{2-} \quad K_1 \qquad (3)$$

$$H^+ + HAsO_4^{2-} = H_2AsO_4^- \quad K_2 \qquad (4)$$

$$H^+ + H_2AsO_4^- = H_3AsO_4^0 \quad K_3 \qquad (5)$$

Values of equilibrium constants, together with their dependence on ionic strength and temperature, were already reported:[46] whereas the first protonation occurs under alkaline conditions, the second takes place at pH $\approx$ 6–7, and the last at very low pH values (*i.e.*, pH $\approx$ 2).

The thermodynamic parameters for the formation of H^+–AsO_4^{3-} species are reported in Table 4 at I = 0.1 mol L^{-1} and T = 298.15 K, chosen as a reference example.[46] As expected for a cation with higher charge, the main contribution to the Gibbs free energy of the first two protonation steps is mainly entropic. In contrast, for the third protonation step, similarly to As^{3+}, the entropic component lowers and it does not represent the highest contribution to the Gibbs free energy.

The effect of ionic strength and temperature is similar to that reported for As^{3+} with a decrease in the formation constants as the above-mentioned parameters increase and a shift of formation curves towards lower pH values. An example of the distribution is reported in Fig. 7 for two different ionic strengths (I = 0.1 and 1 mol L^{-1}) and temperatures (T = 298.15 and 310.15 K). The distribution is in fairly good agreement with the presented *ab initio* molecular dynamics results, according to which under conditions defined as "mild" and "high" (see previous section) the most stable species is $H_2AsO_4^-$, whereas a further increase of the pH will induce the formation of $HAsO_4^{2-}$ and AsO_4^{3-}.

Table 4 Thermodynamic protonation parameters[a] for $AsO_4^{3-}H^+$ species in NaCl at I = 0.1 and at T = 298.15 K

Reaction	log K	ΔH^b	$-\Delta G^b$	$T\Delta S^b$
$H^+ + AsO_4^{3-} = HAsO_4^{2-}$	11.08	−18.1	63.0	44.9
$H^+ + HAsO_4^{2-} = H_2AsO_4^-$	6.62	−6.3	37.8	31.5
$H^+ + H_2AsO_4^- = H_3AsO_4^0$	2.13	−5	12.6	8

[a] Ref. 46. [b] In kJ mol^{-1}.

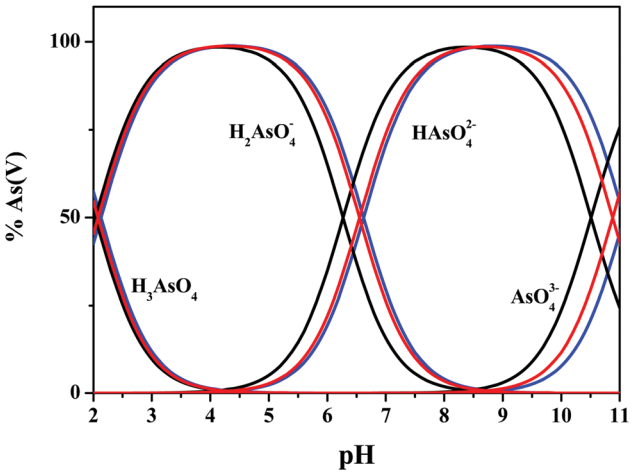

Fig. 7 Distribution diagram for As^{5+} species in NaCl under different experimental conditions (C_M = 1 mmol L^{-1}). Blue lines: I = 0.1 mol L^{-1}, T = 298.15 K; red lines: I = 1 mol L^{-1}, T = 298.15 K; black lines: I = 0.1 mol L^{-1}, T = 310.15 K.

5. Conclusion

In this work, the behaviour of arsenic species in aqueous solutions under different conditions has been explored. In particular, *ab initio* molecular dynamics simulations and experiments have been exploited in a complementary fashion in order to investigate at different scales the hydrolytic behaviour of the most widespread arsenic forms: As^{3+} and As^{5+}.

Our first-principles molecular dynamics calculations have revealed that, under standard conditions, the characteristic time of the third hydrolysis step of As^{3+} – leading to the synthesis of the stable arsenous acid (H_3AsO_3) – statistically falls at 28 ps, a value under-estimated by QM/MM simulations (*i.e.*, 12 ps).[15] On the other hand, in the presence of a very few hydroxide ions τ_3 decreases by more than one order of magnitude and the stable hydrolytic species formed by As^{3+} under strong alkaline conditions is di-hydrogen arsenite ($H_2AsO_3^-$). Although a further hydrolysis step is intuitively expected at higher levels of alkalinity, even under extreme pH conditions no hydrogen arsenite ($HAsO_3^{2-}$) compounds have been detected. This finding has been confirmed by potentiometric and calorimetric measurements where, by sizably varying the pH of the solution, only a single hydrolysis step is observed. In this way, it has been possible to quantitatively define the strength of the interaction through the equilibrium constant (K) and the enthalpy and entropy changes (ΔH, $T\Delta S$) in aqueous solution, and the species distribution *vs.* pH. In particular, As^{3+} is present as arsenous acid up to pH $\approx$ 9 whereas its anion $H_2AsO_3^-$ represents the stable species for 9 $<$ pH $\leq$ 11.

The behaviour of As^{5+} is completely different from that exhibited by As^{3+}. In fact, whereas arsenic acid (H_3AsO_4) species is the most stable under standard conditions, it is involved up to three protonation steps depending on the strength of the alkaline environment. In fact, qualitatively from the present *ab initio* molecular dynamics simulations and quantitatively from the experiments, it turned out that di-hydrogen arsenate

($H_2AsO_4^-$) represents the most stable species for $3 \leq pH \leq 6$ whereas, for $pH > 6$, other two species are produced: hydrogen arsenate ($HAsO_4^{2-}$) and the arsenate anion (AsO_4^{3-}).

In summary, by joining state-of-the-art computational approaches and traditional experiments, we have identified and thermodynamically defined the stable hydrolytic species formed by the most widespread arsenic elements (*i.e.*, As^{3+} and As^{5+}) under conditions thoroughly found in natural waters and in common biological fluids, where the specific chemical coordination of arsenic influences its further interactions with other additional components. The assessment of the form and the stability in which arsenic cations lie under certain conditions is of crucial relevance in the transport, uptake, biological, and physiological mechanism of action of these species in aqueous media. Understanding of the latter is necessary not only to determine the risks of human exposure to this compound but also to predict its medical properties. In particular, modeling the reactivity of arsenic species is fundamental for medical and therapeutic applications, ultimately contributing to the identification of the best experimental conditions for the deployment of arsenic-based compounds in cancer therapy.

Conflicts of interest

There are no conflicts to declare.

Acknowledgements

G. C. thanks Dr Holger Kruse for useful discussions. C. F. and O. G. thank MIUR (Ministero dell'Istruzione, dell'Università e della Ricerca) for financial support (co-funded PRIN project with Prot. 2015MP34H3) whereas D. C. thanks FSE regional funds for PhD support.

References

1 E. Merian, M. Anke, M. Ihnat and M. Stoeppler, *Elements and their compounds in the environment*, Wiley-VCH Verlag GmbH & Co., Weinheim, 2004.
2 A. Sigel, H. Sigel and R. K. O. Sigel, *Interrelations between Essential Metal Ions and Human Diseases*, Springer, 2013.
3 V. K. Sharma and M. Sohn, *Environ. Int.*, 2009, **35**, 743–759.
4 J. Ng, *Environ. Chem.*, 2005, **2**, 46–60.
5 M. Bissen and F. H. Frimmel, *Acta Hydrochim. Hydrobiol.*, 2003, **31**, 9–18.
6 P. L. Smedley and D. G. Kinniburgh, *Appl. Geochem.*, 2002, **17**, 517–568.
7 B. K. Mandal and K. T. Suzuki, *Talanta*, 2002, **58**, 201–235.
8 A review of human carcinogens. Part C: Arsenic, metals, fibres, and dusts, *IARC monographs on the evaluation of carcinogenic risks to humans*, International Agency for Research on Cancer, Lyon, France, 2009.
9 S. J. S. Flora, *Handbook of Arsenic Toxicology*, Academic Press, 2015.
10 I. Khairul, Q. Q. Wang, Y. H. Jiang, C. Wang and H. Naranmandura, *Oncotarget*, 2017, **8**, 23905–23926.
11 N. Saint-Jacques, L. Parker, P. Brown and T. J. Dummer, *Environ. Health*, 2014, **13**, 44.
12 S. J. Ralph, *Met.-Based Drugs*, 2008, 260146.
13 B. Desoize, *Anticancer Res.*, 2004, **24**, 1529–1544.
14 K. Rehman and H. Naranmandura, *Curr. Drug Metab.*, 2013, **14**, 1029–1041.
15 Y. Xu, B. Ma and R. Nussinov, *J. Phys. Chem. B*, 2012, **116**, 4801–4811.
16 A. Sattar, S. Xie, M. A. Hafeez, X. Wang, H. I. Hussain, Z. Iqbal, Y. Pan, M. Iqbal, M. A. Shabbir and Z. Yuan, *Environ. Toxicol. Pharmacol.*, 2016, **48**, 214–224.
17 S. Shen, Xing-Fang Li, W. R. Cullen, M. Weinfeld and X. Chris Le, *Chem. Rev.*, 2013, **113**, 7769–7792.
18 B. Chen, Q. Liu, A. Popowich, S. Shen, X. Yan, Q. Zhang, X. Li, M. Weinfeld, W. R. Cullen and X. C. Le, *Metallomics*, 2015, **7**, 39–55.
19 H. Kaur, R. Kumar, J. N. Babu and S. Mittal, *Biosens. Bioelectron.*, 2015, **63**, 533–545.
20 L. R. Canaval, O. M. D. Lutz, A. K. H. Weiss, C. W. Huck and T. S. Hofer, *Inorg. Chem.*, 2014, **53**, 11861–11870.
21 A. M. Saitta, F. Saija and P. V. Giaquinta, *Phys. Rev. Lett.*, 2012, **108**, 207801.
22 G. Cassone, P. V. Giaquinta, F. Saija and A. M. Saitta, *J. Phys. Chem. B*, 2014, **118**, 12717–12724.
23 G. Cassone, F. Creazzo, P. V. Giaquinta, J. Sponer and F. Saija, *Phys. Chem. Chem. Phys.*, 2017, **19**, 20420–20429.
24 G. Cassone, G. Calogero, J. Sponer and F. Saija, *Phys. Chem. Chem. Phys.*, 2018, **20**, 13038–13046.
25 T. S. Hofer, M. Hitzenberger and B. R. Randolf, *J. Chem. Theory Comput.*, 2012, **8**, 3586–3595.
26 A. Bhattacharjee, T. S. Hofer, A. B. Pribil, B. R. Randolf and B. M. Rode, *Chem. Phys. Lett.*, 2009, **473**, 176–178.
27 J. Hutter, M. Iannuzzi, F. Schiffmann and J. VandeVondele, *WIREs Comput. Mol. Sci.*, 2014, **4**, 15–25.
28 A. D. Becke, *Phys. Rev. A: At., Mol., Opt. Phys.*, 1988, **38**, 3098.
29 C. Lee, W. Yang and R. G. Parr, *Phys. Rev. B: Condens. Matter Mater. Phys.*, 1988, **37**, 785.
30 S. Grimme, J. Antony, S. Ehrlich and H. Krieg, *J. Chem. Phys.*, 2010, **132**, 154104.
31 S. Grimme, S. Ehrlich and L. Goerigk, *J. Comput. Chem.*, 2011, **32**, 1456.
32 S. Goedecker, M. Teter and J. Hutter, *Phys. Rev. B: Condens. Matter Mater. Phys.*, 1996, **54**, 1703–1710.
33 G. Bussi, D. Donadio and M. Parrinello, *J. Chem. Phys.*, 2007, **126**, 014101.
34 C. De Stefano, S. Sammartano, P. Mineo and C. Rigano, Computer Tools for the Speciation of Natural Fluids, in *Marine Chemistry – An Environmental Analytical Chemistry Approach*, ed. A. Gianguzza, E. Pelizzetti and S. Sammartano, Kluwer Academic Publishers, Amsterdam, 1997, pp. 71–83.
35 L. Alderighi, P. Gans, A. Ienco, D. Peters, A. Sabatini and A. Vacca, *Coord. Chem. Rev.*, 1999, **184**, 311–318.
36 O. Coskuner and T. C. Allison, *Chem. Phys. Chem.*, 2009, **10**, 1187–1189.

37 G. Cassone, F. Pietrucci, F. Saija, F. Guyot and A. M. Saitta, *Chem. Sci.*, 2017, **8**, 2329–2336.
38 G. Cassone, F. Petrucci, F. Saija, F. Guyot, J. Sponer, J. E. Sponer and A. M. Saitta, *Sci. Rep.*, 2017, **7**, 6901.
39 D. K. Nordstrom and J. Majzlan, *Rev. Mineral. Geochem.*, 2014, **79**, 217–255.
40 P. Cardiano, D. Chillè, C. Foti and O. Giuffrè, *Fluid Phase Equilib.*, 2018, **458**, 9–15.
41 P. Cardiano, C. Foti and O. Giuffrè, *J. Mol. Liq.*, 2016, **223**, 360–367.
42 P. Cardiano, C. Foti and O. Giuffrè, *J. Mol. Liq.*, 2017, **240**, 128–137.
43 D. Chillè, C. Foti and O. Giuffrè, *J. Chem. Thermodyn.*, 2018, **121**, 65–71.
44 C. Bretti, C. De Stefano, C. Foti, O. Giuffrè and S. Sammartano, *J. Solution Chem.*, 2009, **38**, 1225–1245.
45 C. Foti, O. Giuffrè and S. Sammartano, *J. Chem. Thermodyn.*, 2013, **66**, 151–160.
46 D. Chillè, C. Foti and O. Giuffrè, *Chemosphere*, 2018, **190**, 72–79.

